Malaysian Journal of Chemistry, 2025, Vol. 27(3), 38-47
(Special Issue: *2nd International Science and Technology Colloquium, i-COSTECH 2024*)

Preparation of Silver Phosphate/Graphitic Carbon Nitride via Microwave Irradiation for Photodegradation of Rhodamine B

Halim, O. M.[1]*, Haslinda, H.[1], Ahmad, Z.[1], Nawawi, W. I.[1], Tan, K. H.[2], Jamaluddin, N.[3], Izzudin, N. M.[4], Jalil, A. A.[4], Azmi, A. A.[5] and Azami, M. S.[1]*

[1]Faculty of Applied Sciences, Universiti Teknologi MARA, 02600 Shah Arau, Perlis, Malaysia
[2]Centre for Advanced Materials, Faculty of Engineering and Technology, Tunku Abdul Rahman University of Management and Technology, 53300 Kuala Lumpur, Malaysia
[3]Faculty of Science, Universiti Teknologi Malaysia, 81310 UTM Johor Bahru, Johor, Malaysia
[4]School of Chemical and Energy Engineering, Faculty of Engineering, Universiti Teknologi Malaysia, 81310 UTM Johor Bahru, Johor, Malaysia.
[5]Malaysia Japan International Institute of Technology, University Teknologi Malaysia, 54100 Kuala Lumpur, Wilayah Persekutuan Kuala Lumpur, Malaysia
*Corresponding author (e-mail: saifulddin@uitm.edu.my)

Silver phosphate – AP; (Ag_3PO_4)/Graphitic carbon nitride – CN; (g-C_3N_4) catalysts are successfully synthesized via a facile solid-state microwave-assisted method under various loadings of g-C_3N_4 and then characterized by XRD, FTIR, FESEM and UV-Vis DRS analysis. The catalytic activity towards visible-light photodegradation of rhodamine B is of the following order: 10wt% CNAP (95%) > 5wt% CNAP (82%) > silver phosphate (68%) > 15wt% CNAP (54%) > Graphitic carbon nitride (50%). The highest activity of 10wt% CNAP is due to the synergistic impact of C and N in the C_3N_4 has contributed considerably to the highest number of defect sites. These features lowered the band gap energy which induces the charge carrier recombination. Consequently, photogenerated holes play a crucial role in the degradation as proved by a scavenger study. It is believed that the type-II heterojunction of CNAP has effectively achieved and demonstrates an excellent alternative to photocatalytic degradation to encounter most wastewater issues.

Keywords: Silver phosphate; graphitic carbon nitride; photocatalysis; RhB dye; microwave irradiation

Received: September 2024; Accepted: December 2024

Rhodamine B (RhB) is a synthetic dye that is commonly utilized in industries. Specifically, RhB dyes can pose a major ecological impact even at low concentrations due to the complex xanthene class chemical structure and lead to higher water solubility in the water stream [1]. Thus, the effective environmental treatment to remove RhB needs further consideration. As a consequence, wide alternatives have been reported such as absorption [2], electrocatalytic [3], and sonochemical methods [4]. However, most of these treatments face certain drawbacks, including the possibility of secondary products, costly, time-consuming, and less efficient to complete decolorization of dyes [5].

Heterogeneous photocatalysis with semiconductors such as Ag_3PO_4, TiO_2, CdS, ZnO, ZnS, and Fe_2O_3, leads to the mineralization of organic pollutants. Ag_3PO_4 is widely acknowledged by many researchers as a leading photocatalyst for organic pollutants due to its strong capacity to degrade most of the model pollutants, chemical stability, and low cost with ambient operating conditions. Furthermore, the appropriate band gap energy of Ag_3PO_4 towards g-C_3N_4 which stands to maintain the redox ability for the photogenerated electron holes [6,7]. Theoretically, Ag_3PO_4 has narrow band gap energy of approximately 2.36 – 2.45 eV. Notwithstanding, it has some limitation where the poor active sites and low surface area [8]. As a result, several approaches have been recognized to encounter the limitation by modifying the morphology and coupling with other semiconductors to construct heterojunctions which can increase the surface area, and active sites as well as enhance the photocatalytic activity.

Recently, graphitic carbon nitride (g-C_3N_4), is considered a suitable photocatalyst due to the lower band gap energy around 2.7eV, high chemical stability, low cost, and non-toxic which is environmentally friendly [9-11]. The unique characteristics of g-C_3N_4 help to demonstrate effective interfacial contact of the photocatalyst between Ag_3PO_4 and g-C_3N_4 as well as to have an extraordinary effect on photocatalytic activity. In addition, g-C_3N_4 has soft polymeric structures that can be easily coated on the core-shell structure of the Ag_3PO_4 surface [12]. At the interface of these two photocatalysts, it interacts with the electric field which reduces the recombination and could enhance the charge transfer efficiency of photogenerated electron-hole pairs [13].

†Paper presented at the 2nd International Science and Technology Colloquium (i-COSTECH 2024)

Hence, in this work, we report a facile solid-state microwave-assisted method to synthesize g-C_3N_4 loaded on the Ag_3PO_4 for the photocatalytic reaction of RhB. The heating effect with microwave irradiation promoted the high crystallinity, improved the morphology, and achieved higher phase purity to increase the photocatalytic performance in this study [14]. Furthermore, the combination of these two photocatalysts plays dual function roles narrowing the band gap and mediating the type-II heterojunction charge separation. The photodegradation of RhB was conducted under the illumination of visible light. The kinetic and optimization study of the prepared photocatalyst is also being discussed. Based on the few characterizations study and scavenger test. The proposed mechanism of the photodegradation towards RhB dyes also was illustrated. Thus, we believe that this composite photocatalyst of Ag_3PO_4/g-C_3N_4 will allow the viable strategy for the heterojunction formation and encounter most of the wastewater problems for the industries.

MATERIALS AND METHODS

Chemicals and Materials

Certain chemicals such as disodium hydrogen phosphate anhydrous (Na_2HPO_4), silver nitrate ($AgNO_3$), urea ($CO(NH_2)_2$; with purity 99%), rhodamine B (RhB; with purity 99%– C.I No. 45170; M.W-479.02 g/mol; λmax – 555nm), and methanol were purchased from Malaysia (Merck Sdn Bhd), potassium iodide (KI), toluene, potassium chlorate was purchased from Malaysia (Thermo Scientific Sdn Bhd), sodium hydroxide (NaOH), isopropanol, and butanol were purchased from Malaysia (HmbG Chemicals). The pH solution was altered by using HCl, deionized water, and NaOH solution.

Synthesis of g-C_3N_4

A simple pyrolysis system was used to prepare g-C_3N_4. A certain amount of urea was calcined at 550 ℃ for 2 h under the furnace. Once the pyrolysis was complete, the prepared catalysts were cooled down until room temperature. As a result, the yellow chunk of g-C_3N_4 was ground to form a fine further for further usage [15].

Synthesis of Ag_3PO_4

The preparation of silver phosphate (Ag_3PO_4) was prepared using the precipitation method. 0.5 g of disodium hydrogen phosphate anhydrous (Na_2HPO_4) was dissolved in 10 mL of distilled water (solution A). Meanwhile, 1.5 g of silver nitrate ($AgNO_3$) was dissolved in 40 mL of distilled water with continuous stirring for 30 min (solution B). The solution A was mixed with solution B and stirred for 2 h. Then, the yellow precipitation was collected and dry for 4 h at 110 ℃ [16].

Synthesis of Ag_3PO_4/g-C_3N_4

The facile solid-state method under microwave irradiation was used to prepare the composite catalyst of Ag_3PO_4/g-C_3N_4 [17]. The appropriate amount of Ag_3PO_4 and g-C_3N_4 were mixed in 50 mL of distilled water. The mixed catalyst then was dried for 2 h at 110 ℃. The dry yellow solid was placed in the microwave for 30 min at 450 W. The Ag_3PO_4 weight loading is in the range of 1-15 wt. % was investigated and labeled as x- CNAP, specifically as 5 CNAP, 10 CNAP, and 15 CNAP.

Photodegradation of RhB

The photocatalytic reaction of RhB was investigated in the glass cell with the dimension 50 mm width × 10 depth × 80 height and irradiated with a 20 W (LED lamp where λ = 200 -380 nm). An aquarium pump model NS 7200 was used as an aeration source for the supply of oxygen. For the purpose to accomplish the equilibrium of adsorption-desorption, the reaction solution was conducted in the dark conditions around 1 h. The pH solution is at pH=5 and initial concentration of RhB at 10 mg L^{-1}.

Characterization Methods

The phase of the catalyst was measured using X-ray diffractometer (XRD) by utilizing the instrument of ADVANCE Bruker D8 in the range 2θ = 3º to 90º. In addition, the morphological behavior of the catalyst was evaluated through Field-emission scanning electron microscope (FESEM) with instrument brand no. JEOL JSM-6701F while the functional group and chemical characteristics of the synthesized photocatalyst was observed using Fourier transform infrared (FTIR) spectrometer with Agilent Cary 640 via KBr procedure. In order to verify the band gap and optical absorption analysis, it was characterized by using Agilent Cary 60 UV-Vis/drs spectrophotometer with plotting Kubelka Munk (K-M).

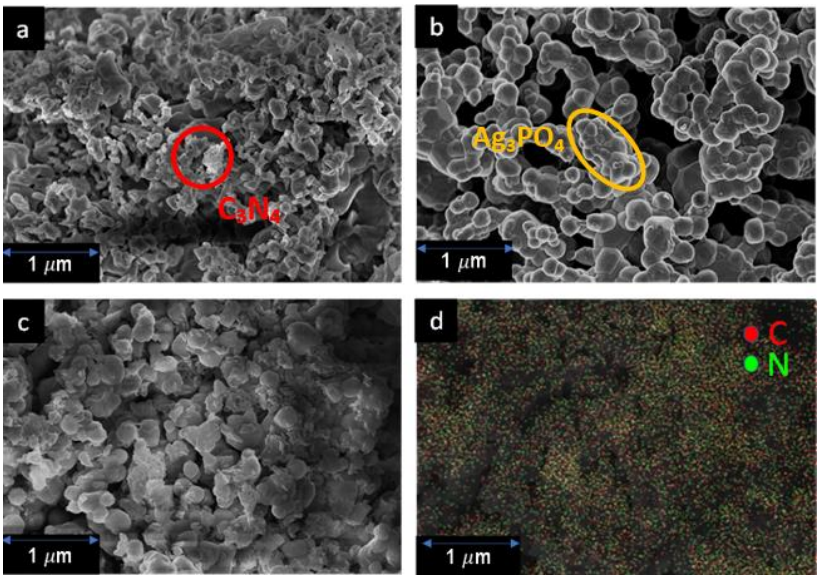

Figure 1. (a) FESEM image of C_3N_4;(b) Ag_3PO_4;(c)10 CNAP;(d) Element mapping of C and N for 10 CNAP.

RESULTS AND DISCUSSION

Physicochemical studies of Ag_3PO_4/g-C_3N_4 Photocatalyst

Surface Microscopic Study

The surface morphology of the catayst was examined by FESEM as depicted in **Figure 1**. Noticeable, two-dimensional lamellar structure was clearly visible (**Figure 1a**), which is the typical characteristic structure of g-C_3N_4 as synthesized by the polymerization method [18]. Meanwhile, the Ag_3PO_4 photocatalyst (**Figure 1b**) demonstrated a uniform particle size and a well-ordered irregular shape morphology. The uniform microbubble surface of Ag_3PO_4 provides a high surface area that can increase the efficiency of photocatalytic degradation of model pollutants [19]. For 10CNAP composites illustrated in **Figure 1c**, a large amount of well-defined of both catalyst between Ag_3PO_4 and g-C_3N_4 can be found even low concentrations loaded. From the elemental mapping of C and N for the 10CNAP composites as shown in **Figure 1d**, it can be indicate that both of this element are randomly distributed in each of the Ag_3PO_4 surface. As previously studied by researchers, this suggests present that the Ag_3PO_4 surface is uniformly loaded with C and N on g-C_3N_4. It is anticipated that the well-dispersed contact of Ag_3PO_4 on the surface of g-C_3N_4 will increase the amount of visible light absorbed during photocatalysis [20].

Structural and Phase Study

The XRD patterns of the g-C_3N_4, and as-prepared 10wt% Ag_3PO_4/g-C_3N_4 (10CNAP) were determined using diffractogram of XRD in the wide range of angle, as can be seen in **Figure 2**. There is a main characteristic peak at $2\theta = 27.52°$ in the XRD pattern of g-C_3N_4, which correspond to the (0 0 2) planes that related with the conjugated aromatic system of the inter-planar stacking (JCPDS 87-1526). Meanwhile, all diffraction peaks of the as-prepared 10CNAP at the $2\theta = 20.89°$, 29.71°, 33.32°, 36.59°, 42.486°, 47.81°, 52.68°, 55.02°, 57.29°, 61.64°, 65.84°, 69.93°, 71.88°, 73.87° and 77.74° which indexed as a (1 1 0), (2 0 0), (2 1 0), (2 1 1), (2 2 0), (3 1 0), (2 2 2), (3 2 0), (3 2 1), (4 0 0), (3 3 0), (4 2 0), (4 2 1), (3 3 2), and (4 2 2) crystal phase of cubic Ag_3PO_4 (JCPDS 06-0505), respectively [21]. Even though, the small portion of 10 wt% Ag_3PO_4 loaded on the g-C_3N_4, the peak still present and can be correlated with the well dispersion that is proved by FESEM which give the concrete evidence that both photocatalyst has successfully composited [22].

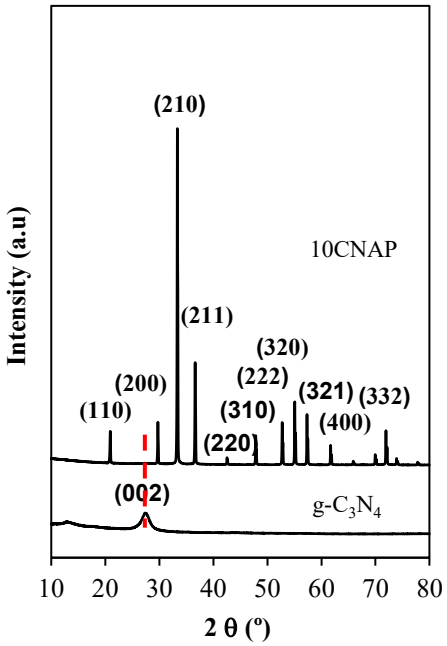

Figure 2. X-ray diffraction patterns of g-C_3N_4 and 10CNAP.

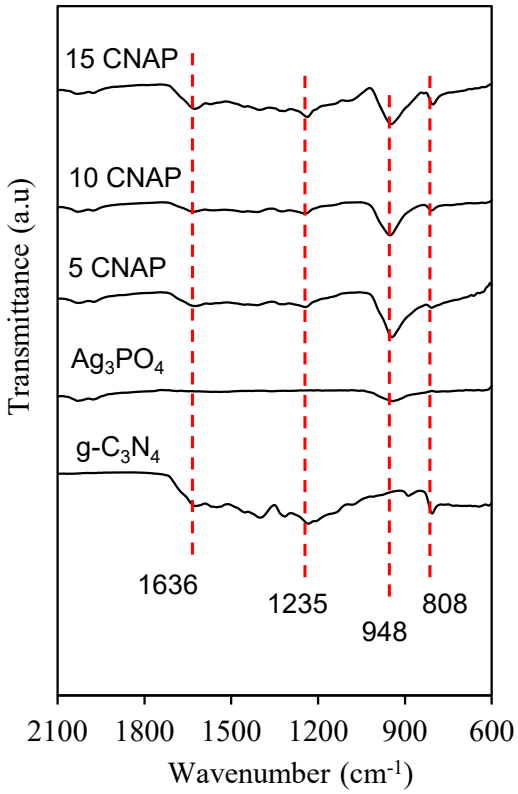

Figure 3. FTIR Spectra of Ag_3PO_4, g-C_3N_4, 5 CNAP,10 CNAP and 15 CNAP.

Vibrational Spectroscopy

The FTIR spectra for the prepared photocatalyst were determined in the range of 2100-600 cm^{-1} as shown in **Figure 3**. It shown that there are two absorption bands that derive from the main peaks of g-C_3N_4 was observed at 1636 and 1235 cm^{-1}. It is assigned to the C-N stretching vibration mode and C-N heterocycle of aromatic, respectively [23]. Generally, the strong absorption bands in the 1200~1650 cm^{-1} region were ascribed to the typical skeletal stretching vibration modes of the s-triazine or tri-s-triazine, which corresponded to the CN heterocycles [24]. Meanwhile, the sharp peak centered at 808 cm^{-1} indicated a characteristic

breathing mode of the triazine units. For the Ag_3PO_4 shows there is a minor peak at 948 cm^{-1} which corresponding to the P-O stretching vibrations of PO_4^{3-} [24]. The CNAP photocatalysts show the successful combination of the Ag_3PO_4 and g-C_3N_4 using microwave irradiation method. However, the intensity of the peak P-O stretching vibration in the CNAPs was more intense as compared to its parent g-C_3N_4 catalyst. This might be due to the g-C_3N_4 could increase the interaction of interlayer in the Ag_3PO_4 [25]. In addition, the incorporation of Ag_3PO_4 with 10 wt.% of g-C_3N_4 led to a drastic decline in the band intensity, which indicates the strong interaction. This outcome is aligned with the good dispersion of both photocatalyst as confirmed by the FESEM mapping in **Figure 1(c)** and **Figure 1(d)**.

Optical Properties

The UV-Vis/DRS spectroscopy was utilized to measure the optical properties of prepared photocatalyst as depicted in **Figure 4**. The band gap of the catalyst was calculated by Kubelka Munk based on the coefficients of absorption defined as a purpose of incident photon energy as stated in the Equation (1):

$$(\alpha hv)^2 = A\,(hv - Eg) \quad (1)$$

Where α is the absorption coefficient (cm^{-1}), A is a constant, hv is energy excitation (eV) and Eg is the band gap energy [26,27]. As determined in **Figure 4**, the extrapolation slope on the photon energy actually contributes to the value of band gap energy of photocatalyst. It showed that the band gap of unmodified photocatalyst, g-C_3N_4 was measured approximately at 2.70 eV while the band gap of Ag_3PO_4 is 2.20eV which is slightly lowered compared to previous study which is 2.45 eV [28,29]. Meanwhile, intercepts of coupling semiconductor present extrapolated band gap for 5CNAP, 10CNAP and 15CNAP which are 2.30, 2.05 and 2.40 eV respectively. The broad absorption band of 10 CNAP showed a drastically shift to lower energies from 2.70 eV to 2.05 eV after additional of Ag_3PO_4. This implies that when introduce the Ag_3PO_4 in g-C_3N_4, the band gap was reduced and led to a good utilization rate in visible light with efficient generation of electron-hole pairs. This will improve the ability of photocatalyst to harvest which favors the higher photocatalytic performance [30].

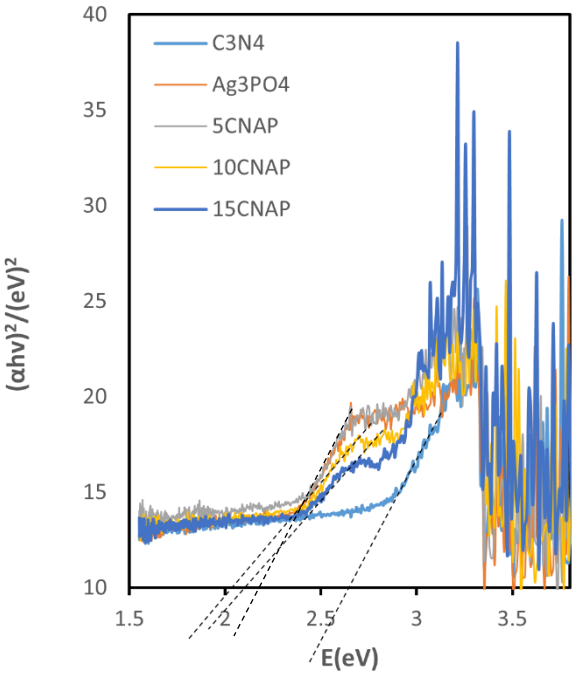

Figure 4. UV-Vis diffuse reflectance spectra of the prepared photocatalyst.

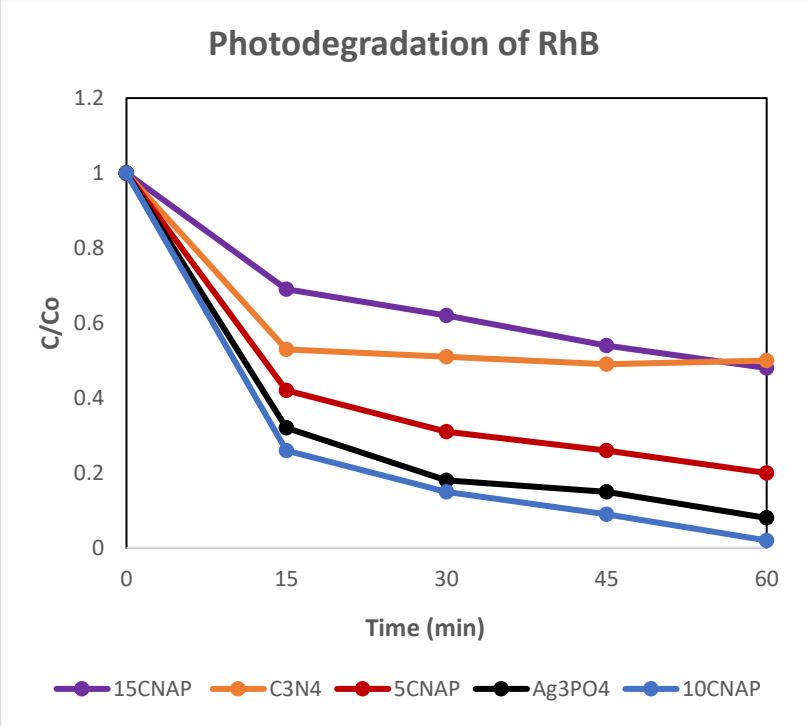

Figure 5. Photodegradation of RhB under visible-light irradiation for g-C_3N_4, Ag_3PO_4, 5CNAP, 10CNAP and 15CNAP.

Photocatalytic Activity of the Ag_3PO_4/g-C_3N_4

The photocatalytic activity of the CNAP catalyst was investigated on the degradation of RhB under visible light for 60 min and the results are illustrated in **Figure 5**. As evidence, it obviously proved that 10CNAP has the highest degradation rate (95%) followed by 5 CNAP (82%), Ag_3PO_4 (68%), 15 CNAP (54%) and g-C_3N_4 (50%). For the higher performance of 10 CNAP, the synergistic impact of C and N in the C_3N_4 has contributed considerably to the highest number of defect sites and resulted in the lowest band gap. According to studies, a good band gap and defect location would enhance the visible light harvesting, hence boosting the oxidation of organic pollutants [31]. The same incidence was described for the enhanced photodegradation of 2-CP using fibrous silica titania with g-C_3N_4 toward the efficient Z-scheme heterojunction. The strong interaction and well dispersion from 10 CNAP also could give a significant effect for the enhancement of photodegradation of RhB under visible light.

Effect of scavenger for the Ag_3PO_4/g-C_3N_4 Photocatalyst

Next, the 10CNAP heterojunction was selected as the photocatalyst in the photodegradation experiment to further investigate the photocatalytic reaction mechanism of the Ag_3PO_4/C_3N_4 heterojunction. Photogenerated electrons (e-), photogenerated holes (h+), photogenerated hydroxyl radicals absorbed on the catalyst (•OHsurface), and photogenerated hydroxyl radicals absorbed in the bulk solution (•OH bulk) were each scavenged using potassium chlorate, methanol, potassium iodide, and isopropanol, respectively [31]. Noticeably, **Figure 6**, indicates that the photogenerated h^+ (93%) played the most crucial role in the photocatalytic decomposition of RhB, followed by photogenerated e^- (90%) $•OH_{bulk}$ (86%), and $•OH_{surface}$ (73%). The above results verified that the interdependent interaction of C and N on Ag_3PO_4 ,(AP) effectively contributed also to the performance of RhB under visible light [32,33].

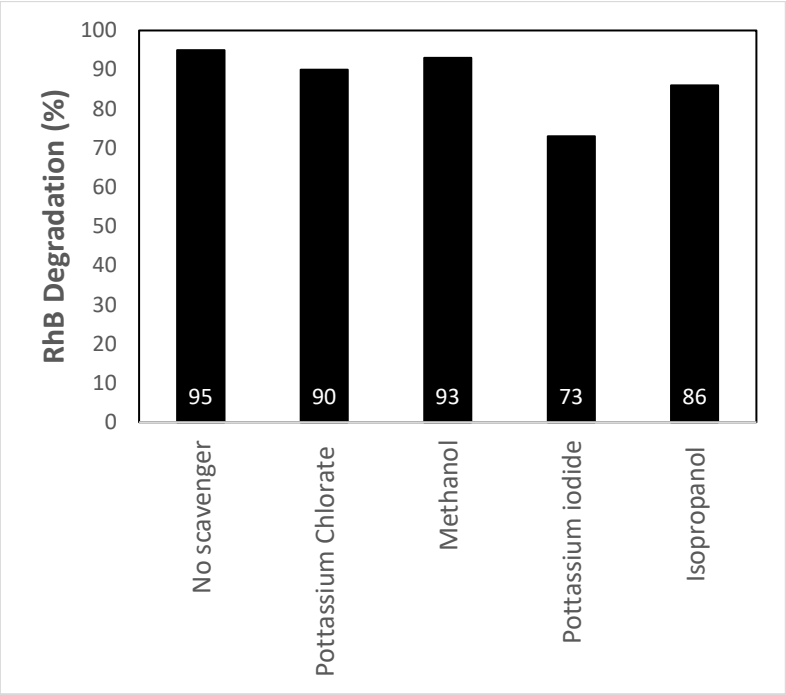

Figure 6. Effects of different scavengers for the RhB photodegradation with 10CNAP under visible-light irradiation.

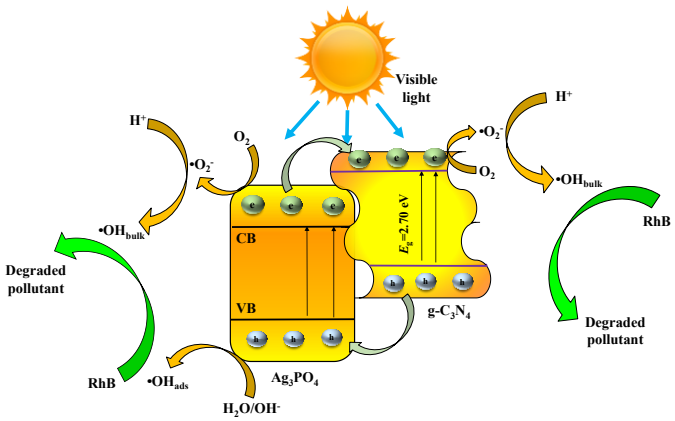

Figure 7. Schematic diagram of the photoexcited electron-hole transfer.

Proposed Mechanism of photocatalytic activity for Ag_3PO_4/g-C_3N_4 Photocatalyst

Based on the above analysis and previous study, a potential Type II Heterojunction mechanism of the CNAP photocatalyst was proposed and schematically illustrated in **Figure 7** [34]. For the Ag_3PO_4, the photogenerated e^- from the valence band (VB) was excited and left positive hole (h^+) at VB before reaching the conduction band (CB). The photogenerated h^+ in Ag_3PO_4 can generate the strong oxidizing agent of hydroxyl radical (•OH) from H_2O, which due to the VB of the Ag_3PO_4 is more positive than the potential level of H_2O/•OH. On the other hand, the VB level of g-C_3N_4 is more negative than the potential level of H_2O/•OH, and therefore, the oxidation of H_2O to •OH by the photogenerated h^+ in the VB of g-C_3N_4 is impossible. Thus, the photogenerated h^+ in the VB g-C_3N_4 will directly migrate to the VB of the Ag_3PO_4. Then, the photogenerated e^- in g-C_3N_4 are trapped by the O_2 in water to form reactive species of superoxide anion radical ($•O_2^-$) as goes to the photogenerated e^- in the CB of the Ag_3PO_4 that possible to convert O_2 into $•O_2^-$ and some part the e^- from Ag_3PO_4 will migrate to the CB of the g-C_3N_4. Fundamentally, the type-II mode, photogenerated holes would accumulate on the VB of PC I with a high oxidation potential whereas photogenerated electrons will collect on the CB of PC II with a low reduction

potential. In this scenario, it may reduce the pushing force toward a certain photocatalytic process. The reluctance from the existing electrons in PC II will obstruct the ongoing flow of electrons from PC I from a dynamic standpoint [35,36]. This type II heterojunction of the photocatalyst could inhibit the recombination of the photogenerated electron-hole.

CONCLUSION

A simple thermal polymeric structure was successfully synthesized g-C_3N_4 by using urea as a precursor while coupling photocatalyst between Ag_3PO_4 and g-C_3N_4 by using solid-state microwave assisted method. The physiochemical behavior of photocatalyst were examined with FESEM, XRD, FTIR and UV-Vis DRS. The highest photodegradation of RhB was demonstrated by 10CNAP (95%) followed by 5 CNAP (82%), Ag_3PO_4 (68%), 15 CNAP (54%) and g-C_3N_4 (50%) under visible light illumination. Low loading of the Ag_3PO_4 was preferred as the optimum due to the highest photocatalytic reaction of 10CNAP. It is because the high interaction of C and N towards the Ag_3PO_4 led to the high number of defect structures. Thus, this defect structure will enhance the efficiency of the interfacial mediator to boost the unique heterojunction formation as well as provide more active sites in the reaction and improve the photogenerated electron holes in 10CNAP photocatalyst. The effect of scavenger proved that the photogenerated holes play an important role in this photocatalytic activity. The photocatalytic degradation of RhB aligned with pseudo-first order of Langmuir-Hinshelwood model and adsorption as controlling step. Hence, this work claimed that the type-II heterojunction between coupling semiconductor with facile solid state microwave irradiation to have impactful and significant as the alternative in the most of photodegradation of numerous model pollutant that meet toward the industrial demands. Despite that, the limitations of the proposed Ag_3PO_4/g-C_3N_4 composite photocatalyst approach primarily involve issues related to surface area, active sites, and recombination of photogenerated carriers, which impact its efficiency in photocatalytic degradation of Rhodamine B (RhB). These limitations imply if the photocatalyst's effectiveness and sustainability for wastewater treatment was applicability without further optimization.

ACKNOWLEDGEMENTS

The authors are grateful for the financial support by the MyRA Research Grant from Universiti Teknologi MARA (UiTM) – Grant No: 600-RMC/GPM LPHD 5/3 (059/2023).

REFERENCES

1. Waghchaure, R. H., Adole, V. A. & Jagdale, B. S. (2022) Photocatalytic degradation of methylene blue, rhodamine B, methyl orange and Eriochrome black T dyes by modified ZnO nanocatalysts: A concise review. *Inorganic Chemistry Communications*, **143**, 109764.

2. Shah, D. V. (2022) Role of Absorption and Adsorption in the Removal of Waste. *CRC Press EBooks*, 33–47.

3. Zhou, X., Yang, J., Guo, J., Xiong, W. & Leung, M. K. H. (2024) Advances and Prospects in Electrocatalytic Processes for Wastewater Treatment. *Processes*, **12(8)**, 1615.

4. Savun-Hekimoğlu, B. (2020) A Review on Sonochemistry and Its Environmental Applications. *Acoustics*, **2(4)**, 766–775.

5. Ahmed, S. F., Mofijur, S. N., Chowdhury, A. T., Rafa, N., Uddin, M. A., Abrar Inayat, T. M. I. Mahlia, Ong, H. C., Chia, W. Y. & Show, P. L. (2021) Recent developments in physical, biological, chemical, and hybrid treatment techniques for removing emerging contaminants from wastewater. *Journal of Hazardous Materials*, **416**, 125912–125912.

6. Wu, R., Song, H., Luo, N., Sheng, Y. & Ji, G. (2018) Microwave-assisted preparation and enhanced photocatalytic activity of Bi_2WO_6/BiOI heterojunction for organic pollutants degradation under visible-light irradiation. *Solid State Sciences*, **87**, 101–109.

7. Zhu, D. & Zhou, Q. (2019) Action and mechanism of semiconductor photocatalysis on degradation of organic pollutants in water treatment: A review. *Environmental Nanotechnology, Monitoring & Management*, **12**, 100255.

8. Li, X., Xu, P., Chen, M., Zeng, G., Wang, D., Chen, F. & Tan, X. (2019) Application of silver phosphate-based photocatalysts: Barriers and solutions. *Chemical Engineering Journal*, **366**, 339–357.

9. Pattanayak, D. S., Pal, D., Mishra, J., Thakur, C. & Wasewar, K. L. (2023) Doped graphitic carbon nitride (g-C_3N_4) catalysts for efficient photodegradation of tetracycline antibiotics in aquatic environments. *Environmental Science and Pollution Research*, **30(10)**, 24919–24926.

10. Wang, L., Wang, K., He, T., Zhao, Y., Song, H. & Wang, H. (2020) Graphitic carbon nitride-based photocatalytic materials: preparation strategy and application. *ACS Sustainable Chemistry & Engineering*, **8(43)**, 16048–16085.

11. Yadav, A. A., Kang, S. W. & Hunge, Y. M. (2021) Photocatalytic degradation of Rhodamine B using graphitic carbon nitride photocatalyst. *Journal of Materials Science: Materials in Electronics*, **32(11)**, 15577–15585.

12. Qi, K., Liu, S. Y., & Zada, A. (2020) Graphitic carbon nitride, a polymer photocatalyst. *Journal of the Taiwan Institute of Chemical Engineers*, **109**, 111–123.

13. Saeed, M., Alwadai, N., Farhat, L. B., Baig, A., Nabgan, W. & Iqbal, M. (2022) Co_3O_4-Bi_2O_3 heterojunction: An effective photocatalyst for photodegradation of rhodamine B dye. *Arabian Journal of Chemistry*, **15(4)**, 103732.

14. Chamoli, P., Shukla, R. K., Bezbaruah, A. N., Kar, K. K. & Raina, K. K. (2021) Microwave-assisted rapid synthesis of honeycomb core-ZnO tetrapods nanocomposites for excellent photocatalytic activity against different organic dyes. *Applied Surface Science*, **555**, 149663.

15. Azami, M. S., Jalil, A. A., Hitam, C. N. C., Hassan, N. S., Mamat, C. R., Adnan, R. H. & Chanlek, N. (2020) Tuning of the electronic band structure of fibrous silica titania with g-C_3N_4 for efficient Z-scheme photocatalytic activity. *Applied Surface Science*, **512**, 145744–145744.

16. Febiyanto, U. S. & Sulaeman, U. (2020) The Starting Material Concentration Dependence of Ag_3PO_4 Synthesis for Rhodamine B Photodegradation under Visible Light Irradiation. *Jurnal Kimia Valensi*, **6(1)**, 1–8.

17. Nguyen, V. H., Pham, A. L. H., Nguyen, V. H., Lee, T. & Nguyen, T. D. (2022) Facile synthesis of bismuth (III) based metal-organic framework with difference ligands using microwave irradiation method. *Chemical Engineering Research and Design*, **177**, 321–330.

18. Samsudin, M. F. R., Bacho, N., Sufian, S. & Ng, Y. H. (2019) Photocatalytic degradation of phenol wastewater over Z-scheme g-C_3N_4/CNT/$BiVO_4$ heterostructure photocatalyst under solar light irradiation. *Journal of Molecular Liquids*, **277**, 977–988.

19. Amiri, F., Dehghani, M., Amiri, Z., Yousefinejad, S. & Azhdarpoor, A. (2021) Photocatalytic degradation of 2, 4-dichlorophenoxyacetic acid from aqueous solutions by Ag_3PO_4/TiO_2 nanoparticles under visible light: kinetic and thermodynamic studies. *Water Science and Technology*, **83(12)**, 3110–3122.

20. Li, J. X., & Xie, Y. L. (2024) Enhanced separation performance of g-C_3N_4/Ag_3PO_4 heterojunction photocatalyst for efficient degradation of methylene blue and bisphenol A. *Journal of Alloys and Compounds*, **1005**, 176115.

21. Shi, W., Li, M., Huang, X., Ren, H., Guo, F. & Yan, C. (2020) Three-dimensional Z-Scheme Ag_3PO_4/$Co_3(PO_4)_2$@ Ag heterojunction for improved visible-light photocatalytic degradation activity of tetracycline. *Journal of Alloys and Compounds*, **818**, 152883.

22. Muhamad, N. A., Rosli, M. A., Hamzah, S. R., Ghani, N. I., Natar, N. S., Azami, M. S., Ishak, M. A., Sabar, S. & Nawawi, W. I. (2024) Aqua-Mediated Hydrothermal Synthesis in the Production of a gC_3N_4/TiO_2 Composite for Photocatalytic Degradation of RR4 Dye. *Malaysian Journal of Chemistry*, **26**, 110–118.

23. Razali, M. H., Md Fauzi, M. A. F., Mohd Azam, B. & Yusoff, M. (2022) g-C_3N_4/TiO_2 nanocomposite photocatalyst for methylene blue photodegradation under visible light. *Applied Nanoscience*, **12(11)**, 3197–3206.

24. Seshadri, M., Batesttin, C., Silva, I. L., Bell, M. J. V. & Anjos, V. (2020) Effect of compositional changes on the structural properties of borophosphate glasses: ATR-FTIR and Raman spectroscopy. *Vibrational Spectroscopy*, **110**, 103137–103137.

25. Mathialagan, A., Manavalan, M., Venkatachalam, K., Mohammad, F., Oh, W. C. & Sagadevan, S. (2020) Fabrication and physicochemical characterization of g-C_3N_4/ZnO composite with enhanced photocatalytic activity under visible light. *Optical Materials*, **100**, 109643.

26. Li, G., Guo, J., Hu, Y., Wang, Y., Wang, J., Zhang, S. & Zhong, Q. (2021) Facile synthesis of the Z-scheme graphite-like carbon nitride/silver/silver phosphate nanocomposite for photocatalytic oxidative removal of nitric oxides under visible light. *Journal of Colloid and Interface Science*, **588**, 110–121.

27. Akhsassi, B., Bouddouch, A., Naciri, Y., Ettahiri, Y., Bakiz, B. A., Taoufyq, S., Villain, F., Guinneton, J., Gavarri, R. & Benlhachemi, A. (2024) Visible light-driven type II p-Bi_3O_4Cl/n-$BiPO_4$ heterojunction for effective photocatalytic photodegradation. *Ceramics International*, **50(18)**, 32338–32352.

28. Nagajyothi, P. C., Sreekanth, T. V. M., Ramaraghavulu, R., Devarayapalli, K. C., Yoo, K., Vattikuti, S. P. & Shim, J. (2019) Photocatalytic dye degradation and hydrogen production activity of Ag_3PO_4/g-C_3N_4 nanocatalyst. *Journal of Materials Science: Materials in Electronics*, **30**, 14890–14901.

29. Moeini, Z., Hoseini, M., Dehghani, M., (2024) Synthesize of heterostructure TiO_2 by simultaneous doping of double silver and phosphate to degradation of methylene blue under visible light. *Applied Water Science*, **14**, 39.

30. Liu, H., Li, D., Yang, X. & Li, H. (2018) Fabrication and characterization of Ag_3PO_4/TiO_2 heterostructure

with improved visible-light photocatalytic activity for the degradation of methyl orange and sterilization of E. coli. *Materials Technology*, **34(4)**, 192–203.

31. Hassan, N. S., Jalil, A. A., Aziz, F. F. A., (2020) Tailoring the Silica Amount in Stabilizing the Tetragonal Phase of Zirconia for Enhanced Photodegradation of 2-Chlorophenol. *Topics in Catalysis*, **63**, 1145–1156.

32. Althamthami, M., Temam, E. G., Temam, H. B., Hasan, G. G. & Malfi, N. (2022) Influence of hole-scavenger and different withdrawn speeds on photocatalytic activity of Co_3O_4 thin films under sunlight irradiation. *Ceramics International*, **48(21)**, 31570–31578.

33. Puga, F., Navío, J. A. & Hidalgo, M. C. (2024) A critical view about use of scavengers for reactive species in heterogeneous photocatalysis. *Applied Catalysis A: General*, **685**, 119879.

34. Azami, M. S., Jalil, A. A., Hassan, N. S., Hussain, I., Fauzi, A. A. & Aziz, M. A. A. (2021) Green carbonaceous material–fibrous silica-titania composite photocatalysts for enhanced degradation of toxic 2-chlorophenol. *Journal of Hazardous Materials*, **414**, 125524–125524.

35. Salazar-Marín, D., Oza, G., Real, J. A. D., Cervantes-Uribe, A., Pérez-Vidal, H., Kesarla, M. K., Torres, J. G. T. & Godavarthi, S. (2023) Distinguishing between type II and S-scheme heterojunction materials: A comprehensive review. *Applied Surface Science Advances*, **19**, 100536–100536.

36. Ren, X., Wu, K., Qin, Z., Zhao, X. & Yang, H. (2019) The construction of type II heterojunction of Bi_2WO_6/BiOBr photocatalyst with improved photocatalytic performance. *Journal of Alloys and Compounds*, **788**, 102–109.